

VI₃: a 2D Ising ferromagnet

Ke Yang,¹ Fengren Fan,¹ Hongbo Wang,² D. I. Khomskii,³ and Hua Wu^{1,4,*}

¹*Laboratory for Computational Physical Sciences (MOE), State Key Laboratory of Surface Physics, and Department of Physics, Fudan University, Shanghai 200433, China*

²*Laboratory of Advanced Materials Physics and Nanodevices, School of Physics and Technology, University of Jinan, Jinan 250022, China*

³*Institute of Physics II, University of Cologne, 50937 Cologne, Germany*

⁴*Collaborative Innovation Center of Advanced Microstructures, Nanjing 210093, China*
(Dated: September 16, 2019)

Two-dimensional (2D) magnetic materials are of great current interest for their promising applications in spintronics. Here we propose the van der Waals (vdW) material VI₃ to be a 2D Ising ferromagnet (FM), using density functional calculations, crystal field level diagrams, superexchange model analyses, and Monte Carlo simulations. The $a_{1g}^1 e'_{-1}$ state in the trigonal crystal field turns out to be the ground state, and it gives rise to the 2D Ising FM due to a significant single ion anisotropy (SIA) associated with the $S_z=1$ and $L_z=-1$ state of V^{3+} ions. Moreover, a tensile strain on the VI₃ monolayer further stabilizes the $a_{1g}^1 e'_{-1}$ ground state, and the enhanced FM superexchange and the strong SIA would raise the Curie temperature of the VI₃ monolayer from 70 K to 90-110 K under a 2.5-5% tensile strain. This prediction is worth a prompt experimental verification.

Two-dimensional (2D) crystals with intrinsic magnetism have been of great interest since the experimental achievements of the atomically thin CrI₃ [1] and Cr₂Ge₂Te₆ [2] flakes by mechanical exfoliation of bulk crystals. Through magneto-optical Kerr effects, the CrI₃ monolayer and Cr₂Ge₂Te₆ atomic layers have been demonstrated to be a ferromagnet (FM) with out-of-plane spin orientation. More recently, isolated monolayers from the layered metallic magnet Fe₃GeTe₂ [3] have been exfoliated and their Curie temperature (T_C) can be above room temperature with ionic gating. Those 2D FMs provide unique opportunities for understanding, exploring and utilizing novel low-dimensional magnetism. Due to the thickness of one or few monolayers, one may be able to control the 2D magnetic properties by applying weak magnetic field [4–6], electric field [4, 5], doping [3, 7], or heterostructure [8, 9]. This flexibility causes enormous excitement about their promising applications in spintronics.

Very recently, VI₃ emerges as a new 2D material with a similar van der Waals (vdW) layered structure as CrI₃ which is currently under extensive study [1, 4–13]. The bulk material of VI₃ has been synthesized by several groups [14–16], and it is found to be an interesting FM insulator with $T_C \approx 50$ K and the easy magnetization c -axis [14, 15]. Note that CrI₃ has a closed t_{2g}^3 shell for the octahedral Cr^{3+} $S=3/2$ ion. Therefore, its orbital singlet produces no single ion anisotropy (SIA), and its finite perpendicular magnetic anisotropy comes from the exchange anisotropy caused predominantly by the spin-orbit coupling (SOC) of the heavy I $5p$ orbitals and their hybridization with the Cr $3d$ [12, 13]. In contrast, VI₃ has an open t_{2g}^2 shell for the $S=1$ V^{3+} , and therefore it has room to achieve an orbital moment and a consequent strong SIA due to SOC. Then, VI₃ may be an Ising type 2D FM.

In this Letter, we indeed find that VI₃ vdW monolayer has the $a_{1g}^1 e'_{-1}$ ground state with $S_z=1$ and $L_z=-1$ in the trigonal crystal field. The FM superexchange and the strong perpendicular SIA produce the 2D Ising FM. The $a_{1g}^1 e'_{-1}$ ground state can further be stabilized by a tensile strain, which would enhance T_C of the VI₃ monolayer from 70 K to 90-110 K under 2.5-5% strain. Therefore, the VI₃ monolayer could be the first real 2D Ising FM, which calls for a prompt experimental verification.

We have carried out density functional theory (DFT) calculations for both bulk and monolayer VI₃, using the full-potential augmented plane wave plus local orbital code (Wien2k) [17]. A 20-Å thick slab was used to model the monolayer. The experimental lattice parameters [14] were used and the structural optimization was also carried out, and two sets of results turn out to be very similar as seen below. The global coordinates are used, with the z -axis parallel to the crystallographic c -axis (i.e., along the [111] direction of the local VI₆ octahedra, see Fig. 1). The muffin-tin sphere radii were chosen to be 2.2 Bohr for V and 2.5 Bohr for I. The plane wave expansion of the interstitial wave functionals was set to be 12 Ry. The Brillouin zone integration was performed over $12 \times 12 \times 1$ k -mesh. To account for the electron correlation of the narrow V $3d$ bands, the local-spin-density approximation plus Hubbard U (LSDA+U) calculations were performed using Hubbard $U=4.0$ eV and Hund exchange $J_H=0.9$ eV [18]. The SOC is included for both V $3d$ and I $5p$ orbitals by the second-variational method. As seen below, the SOC is crucial and any reasonable U (e.g., 2-5 eV) is big enough to open an insulating gap between the SOC split e'_{\pm} states and hence reach the same ground state solution for VI₃. Moreover, we have used the crystal field and superexchange pictures to understand the 2D Ising FM in VI₃ as detailed below. Furthermore, we have estimated the T_C of VI₃ monolayer using Monte Carlo (MC)

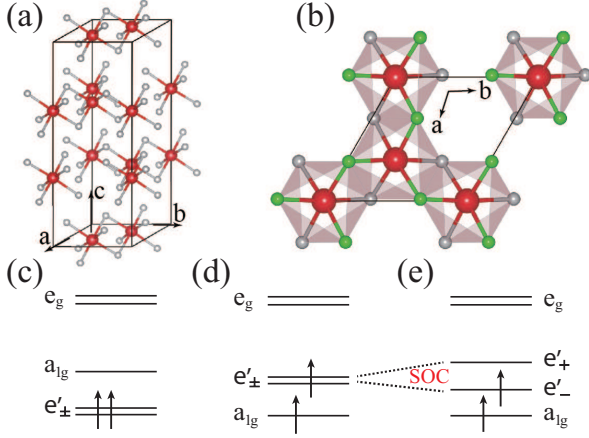


FIG. 1. (a) The bulk crystal structure of VI_3 , with V (I) atoms represented by red (grey) balls. (b) The honeycomb V lattice of VI_3 monolayer, and the green (grey) balls standing for the I atoms above (below) the V layer, forming the edge sharing VI_6 octahedra. (c) The $e'_{\pm}{}^2$ or (d) $a_{1g}{}^1e'_{\pm}{}^1$ configuration for the V^{3+} $S=1$ ion in the trigonal crystal field level diagrams, with the active SOC effect in (e).

simulations on a $6 \times 6 \times 1$ spin matrix. At each temperature, 2.4×10^7 MC steps/site were performed to reach an equilibrium using the Metropolis method [19], and then the specific heat is calculated.

We first consider the situation in the bulk VI_3 where some recent experimental results [14, 15] are available for comparison. According to the crystal structure of the bulk VI_3 in the $R\bar{3}$ space group [14], the V ions have a local octahedral coordination but a trigonal crystal field in the global coordinate system, which splits the otherwise degenerate t_{2g} triplet into the a_{1g} singlet and e'_{\pm} doublet, see Fig. 1. Several very recent DFT studies gave conflicting results for the bulk VI_3 (either metallic [14, 20] or insulating [15, 16]), but so far no understanding of the perpendicular FM has been available. In the DFT+U framework one may readily get the insulating solution with the $e'_{\pm}{}^2$ double occupation, in contrast to the metallic state $a_{1g}{}^1e'_{\pm}{}^1$ with the half filled e'_{\pm} doublet. However, it is the half-filled e'_{\pm} doublet (Figs. 1(d) and 1(e)) which makes the SOC active and may eventually determine the perpendicular FM. For this purpose, we have carried out LSDA+SOC+U calculations for the bulk VI_3 to make a direct comparison between two configurations, $e'_{\pm}{}^2$ and $a_{1g}{}^1e'_{\pm}{}^1$. These two configurations are initialized via the occupation density matrix over the eigen orbitals [21, 22], rather than a common representation by the two doublets (xy , x^2-y^2) and (xz , yz) in the trigonal crystal field, which may not find the correct $a_{1g}{}^1e'_{\pm}{}^1$ ground state in the calculations.

Our LSDA+SOC+U calculations show that both insulating solutions can be stabilized, and that the $a_{1g}{}^1e'_{\pm}{}^1$ state, now with $l_z=-1$, is more stable than the $e'_{\pm}{}^2$ state, by 9.3 meV/fu, as seen in Table I. Both the solutions

TABLE I. Relative total energies ΔE (meV/fu) by LSDA+SOC+U, local spin and orbital moments (μ_B) for the V^{3+} ion. The perpendicular magnetization is assumed in most cases, and the in-plane magnetization is also set for $a_{1g}{}^1e'_{\pm}{}^1$. The corresponding data for the fully relaxed structures are listed in the round brackets.

VI_3 bulk		ΔE	M_{spin}	M_{orb}
$a_{1g}{}^1e'_{\pm}{}^1$	FM	0.0 (0.0)	1.89 (1.86)	-1.05 (-1.00)
	AF	21.3	1.85	-1.07
$a_{1g}{}^1e'_{+}{}^1$	FM	38.7	1.89	1.03
$e'_{\pm}{}^2$	FM	9.3 (11.8)	1.83 (1.80)	0.05 (0.05)
	AF	15.8	1.81	0.07
VI_3 monolayer		ΔE	M_{spin}	M_{orb}
$a_{1g}{}^1e'_{\pm}{}^1$	FM	0.0 (0.0)	1.88 (1.84)	-1.08 (-1.04)
	AF	20.2 (20.0)	1.84 (1.80)	-1.09 (-1.05)
$a_{1g}{}^1e'_{\pm}{}^1$	FM	17.0 (17.6)	1.88 (1.84)	-0.15 (-0.15)
(in-plane M)	AF	35.2 (33.9)	1.84 (1.80)	-0.14 (-0.17)
$e'_{\pm}{}^2$	FM	20.1 (45.5)	1.82 (1.78)	0.05 (0.05)
	AF	27.1 (52.5)	1.80 (1.76)	0.07 (0.07)

have the local V^{3+} spin moment more than $1.8 \mu_B$ and the total spin moment of $2 \mu_B/\text{fu}$, showing exactly the formal V^{3+} $S=1$ state. Note that the former solution has now a large orbital moment of $-1.05 \mu_B$ along the z -axis due to filling of the lower e'_{-} ($l_z=-1$) level after the SOC splitting of the e'_{\pm} doublet (Fig.1(e)). In contrast, the fully occupied $e'_{\pm}{}^2$ doublet has no orbital degree of freedom and thus only a very small orbital moment of $0.05 \mu_B$ is induced by the SOC. To prove the essential role of the SOC, we have also calculated the $a_{1g}{}^1e'_{+}{}^1$ state with filling of the SOC-split upper e'_{+} ($l_z=1$) level. The resulting total energy rises by 38.7 meV/fu, compared with the $a_{1g}{}^1e'_{\pm}{}^1$ ground state. Then the SOC parameter of the V^{3+} ion $\xi=38.7$ meV is derived, and it is (largely) responsible for the energy lowering of the $a_{1g}{}^1e'_{\pm}{}^1$ ground state, relative to the $e'_{\pm}{}^2$ state where the SOC is almost absent. Note that the SOC parameter ξ is partially enhanced [23, 24] here by the strong SOC of the heavy I atom via the I $5p$ -V $3d$ hybridization.

Moreover, for both insulating solutions, $a_{1g}{}^1e'_{\pm}{}^1$ and $e'_{\pm}{}^2$, the FM state is more stable than the antiferromagnetic (AF) state, see Table I. But note that while the FM stability against AF is 6.5 meV/fu for the $e'_{\pm}{}^2$ state, it increases a lot to 21.3 meV/fu for the $a_{1g}{}^1e'_{\pm}{}^1$ ground state. This enhanced FM superexchange in the $a_{1g}{}^1e'_{\pm}{}^1$ ground state appears also in the VI_3 monolayer and will be explained below. The FM order can further be stabilized by its Ising type magnetic moment due to the SOC between the $S_z=1$ and $L_z=-1$. The total magnetic moment of about $1 \mu_B/\text{fu}$ is strongly reduced from the V^{3+} $S=1$ state, and it well accounts for the experimental easy z -axis magnetization of 1-1.3 μ_B in the FM insulat-

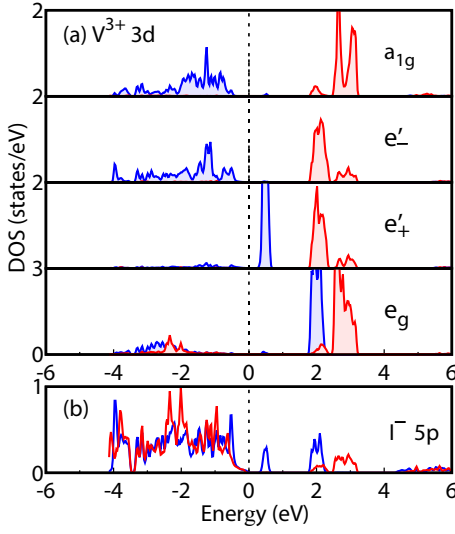


FIG. 2. The $a_{1g}^1 e_{-}^1$ ground state with a strong V 3d-I 5p hybridization by LSDA+SOC+U. The blue (red) curves stand for the up (down) spin. Fermi level is set at zero energy.

ing VI_3 [14, 15].

As VI_3 bulk has already the potential to be an Ising FM, its vdW monolayers could well be a 2D Ising FM, with a better tunability. The cleavage energy is calculated to be 0.27 J/m^2 , using DFT+vdW corrections within the Grimme's approach [25] (see Supplemental Material for details), and it is well comparable to those for other 2D materials such as CrI_3 (0.30 J/m^2) [10], $\text{Cr}_2\text{Si}_2\text{Te}_6$ (0.35 J/m^2) and $\text{Cr}_2\text{Ge}_2\text{Te}_6$ (0.38 J/m^2) [26]. Therefore, an exfoliation of VI_3 monolayer is likely, and we now switch to the treatment of the VI_3 monolayer.

Our LDA and LSDA calculations find a FM metallic solution, and LSDA+U calculations give a FM insulating solution with e_{\pm}^2 , see Supplemental Material for details. One may assume that the experimental FM insulating behavior is reproduced by the e_{\pm}^2 state. However, a key point is the following: the $\text{V}^{3+} e_{\pm}^2$ state has only the pure $S=1$ and a quenched orbital moment, i.e., no SIA which would be very beneficial for the 2D FM. Apparently, such a solution would hardly explain the strong perpendicular FM observed in bulk VI_3 [14, 15]. Then, one may have to resort, as in the extensively studied CrI_3 [12, 13], to the weak exchange anisotropy due to the SOC of I 5p orbital and its strong hybridization with V 3d. But actually, VI_3 has a more than one order of magnitude stronger SIA, which determines its 2D Ising FM as demonstrated below.

Our LSDA+SOC+U calculations give the insulating $a_{1g}^1 e_{-}^1$ ground state (Fig. 2), with the gap opening due to the electron correlation within the SOC-split $t_z = \pm 1$ states, and it is more stable than the e_{\pm}^2 solution by 20.1 meV/fu , see Table I. Note that for the partially-filled t_{2g} systems, there is an old and well-known dichotomy (see, e.g. Ref. 27): such ions, on one hand, are Jahn-Teller

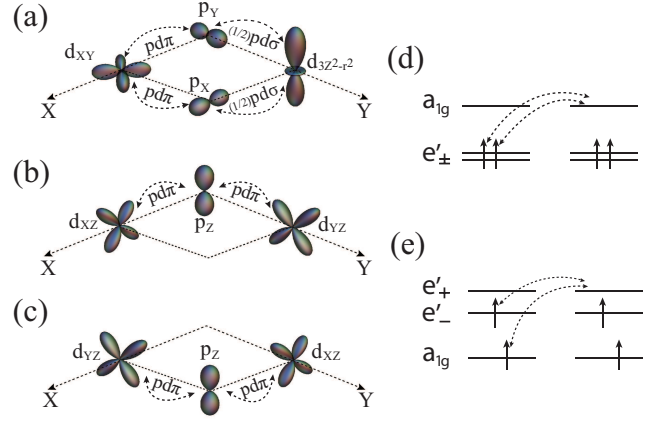


FIG. 3. Schematic plot of the hopping channels involved in the (near-) 90° FM superexchange: (a) $d_{xy} - (p_x, p_y) - d_{3z^2-r^2}$, (b) $d_{xz} - p_z - d_{yz}$, and (c) $d_{yz} - p_z - d_{xz}$. Virtual hoppings between the V^{3+} ions with (d) e_{\pm}^2 and (e) $a_{1g}^1 e_{-}^1$.

(JT) active and may distort and fill orbitals according to the JT scenario - here for $\text{V}^{3+} 3d^2$ occupation, giving the e_{\pm}^2 state. But they can also form the state with unquenched orbital moment and gain extra SOC energy. The above results imply that the SOC effects, from V 3d itself and I 5p via the p - d hybridization (see Fig. 2), indeed favor the $a_{1g}^1 e_{-}^1$ ground state solution.

Moreover, for the $a_{1g}^1 e_{-}^1$ ground state, the FM state is more stable than the AF state by 20.2 meV/fu , which is very similar to the bulk case, see Table I. In contrast, for the e_{\pm}^2 state, the FM state is more stable than the AF state only by 7.0 meV/fu . Here we provide a picture to understand the enhanced FM superexchange in the $a_{1g}^1 e_{-}^1$ ground state. Considering the honeycomb lattice of the V^{3+} magnetic ions and the edge-sharing VI_6 octahedral network (see Fig. 1), we discuss the near- 90° FM superexchange interactions, see Fig. 3. Here we choose a local octahedral XYZ coordinate system, with the XYZ axes directed from V to neighboring I ions. Then the local octahedral t_{2g} triplet under a trigonal crystal field can be expressed as

$$\begin{aligned} a_{1g} &= \frac{1}{\sqrt{3}}(XY + XZ + YZ) \\ e_{+}^1 &= \frac{1}{\sqrt{3}}(XY + e^{i2\pi/3}XZ + e^{i4\pi/3}YZ) \\ e_{-}^1 &= \frac{1}{\sqrt{3}}(XY + e^{i4\pi/3}XZ + e^{i2\pi/3}YZ). \end{aligned} \quad (1)$$

The V-V superexchange contains several contributions. In analogy with the well studied CrI_3 , the main FM contribution comes from the occupied t_{2g} - empty e_g virtual hoppings [11]. There are also AF processes, due to hoppings between the occupied t_{2g} orbitals. Importantly, in VI_3 , and in contrast to CrI_3 , there appear the FM contributions due to hoppings from occupied to empty t_{2g}

orbitals; these will turn out to be crucial in enhancing FM contributions for the $a_{1g}^1 e_{-1}^1$ ground state.

We schematically illustrate these contributions treating VI_3 as a Mott-Hubbard (MH) insulator. Actually for such ligand as I the system may be close to a charge-transfer (CT) regime, see e.g. Ref. 27; this would add extra terms in the superexchange, but this would not change the main conclusions here. In the MH regime the main superexchange occurs due to the effective d - d hoppings through the same $5p$ orbital of I ions (in CT case also the hoppings via different orthogonal $5p$ orbitals could enter). The main FM contribution comes from the effective V-V hopping from each of the above three orbitals to the neighboring empty (real) e_g orbital $3Z^2 - r^2$ via the mechanism shown in Fig. 3(a) (the hoppings to $X^2 - Y^2$ orbital via two iodine ions cancel due to the signs of the d - and p -wave functions). According to Fig. 3(a), only the XY component of each of the states in Eq. 1 is active here, and the hoppings from each of them to the $3Z^2 - r^2$ orbital of a neighboring V are equal, and we see that this FM contribution is the same for both the $a_{1g}^1 e_{-1}^1$ and e_{\pm}^2 configurations.

As mentioned above, also for t_{2g} - t_{2g} contributions, the V-V hopping and superexchange via the common single $5p_z$ orbital of two I⁻ ligands, as sketched in Figs. 3(b) and 3(c), are also effective. Then we have the effective hoppings as follows

$$\begin{aligned} \langle a_{1g} | \hat{t} | a_{1g} \rangle &= -2t_0, & \langle e_{+}^1 | \hat{t} | e_{+}^1 \rangle &= \langle e_{-}^1 | \hat{t} | e_{-}^1 \rangle = -t_0, \\ \langle e_{+}^1 | \hat{t} | e_{-}^1 \rangle &= -2t_0, & \langle a_{1g} | \hat{t} | e_{+}^1 \rangle &= \langle a_{1g} | \hat{t} | e_{-}^1 \rangle = -t_0, \end{aligned} \quad (2)$$

where $t_0 = t_{pd\pi}^2 / (3\Delta)$ and Δ is the charge transfer energy. Using these hoppings, one can show that the AF contribution due to hopping between occupied t_{2g} orbitals is again the same for both $a_{1g}^1 e_{-1}^1$ and e_{\pm}^2 . This is however not the case for the FM t_{2g} - t_{2g} contribution. Then, for the e_{\pm}^2 state (Fig. 3(d)), the FM superexchange due to the above hoppings gains the energy against the AF by $(4t_0^2/U) \cdot (2J_H/U)$. But for the $a_{1g}^1 e_{-1}^1$ ground state (Fig. 3(e)), the corresponding energy gain is more than doubled, $(10t_0^2/U) \cdot (2J_H/U)$. This could be a major reason why the $a_{1g}^1 e_{-1}^1$ ground state has a much enhanced FM superexchange as compared to e_{\pm}^2 , as shown in the above LSDA+SOC+U calculations.

Note that the $a_{1g}^1 e_{-1}^1$ ground state has a local V^{3+} spin moment of $1.88 \mu_B$ and an antiparallel orbital moment of $-1.08 \mu_B$ along the z -axis, i.e., the SOC aligns the magnetic moment along the z -axis via the strong SIA, thus producing the perpendicular magnetic anisotropy and the resulting Ising magnetism. Here we assume the spin Hamiltonian

$$H = -\frac{J}{2} \sum_{i,j} \vec{S}_i \cdot \vec{S}_j - D \sum_i (S_i^z)^2 - \frac{J'}{2} \sum_{i,j} S_i^z \cdot S_j^z, \quad (3)$$

where the first term describes the Heisenberg isotropic exchange (FM when $J > 0$), the second term is the SIA

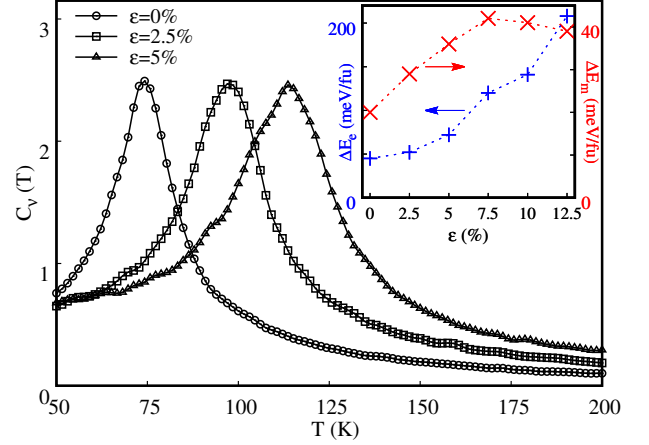


FIG. 4. Monte Carlo simulations of the specific heat of the VI_3 monolayer under tensile strains. The inset shows the relative stability of the $a_{1g}^1 e_{-1}^1$ ground state against the e_{\pm}^2 state (blue curve), and the FM stability of the $a_{1g}^1 e_{-1}^1$ ground state against the AF state (red curve).

with the easy magnetization z axis (when $D > 0$), and the last term refers to the anisotropic exchange (the easy z axis when $J' > 0$). The sum over i runs over all V^{3+} atoms with $S=1$ in the honeycomb lattice, and j over the three first nearest V^{3+} neighbors of each i . We have estimated the three magnetic parameters J , D and J' , by calculating four different magnetic states, FM and AF with the perpendicular or in-plane magnetization, see Table I. The total energy results allow us to estimate $J=6.07$ meV, $D=15.9$ meV, and $J'=0.67$ meV. We see that the perpendicular magnetic anisotropy of the VI_3 monolayer arises predominantly from the D -term, i.e., from the strong Ising-type SIA. This is one of the main results of this Letter. With these three parameters, our Monte Carlo simulations find that T_C of the VI_3 monolayer would be 40 K with the J - J' contributions, 68 K with the J - D contributions, and 74 K with the J - D - J' contributions. Therefore, the D contribution is about 5 times stronger than J' in stabilizing the 2D FM order.

The above results remain largely unchanged when we carry out a structural optimization for the VI_3 monolayer, see Table I. The only significant change is that the insulating $a_{1g}^1 e_{-1}^1$ ground state, at the theoretical equilibrium lattice constant $a=b=6.70$ Å (as compared with the experimental bulk value $a=b=6.88$ Å [14]), becomes even more stable than the e_{\pm}^2 state, by 45.5 meV/fu. Actually, the more stable $a_{1g}^1 e_{-1}^1$ ground state is preferable for the VI_3 monolayer, and it determines the Ising FM desirable for 2D materials. As we demonstrate below, this goal can be achieved when a biaxial tensile strain is exerted on the VI_3 monolayer. With the tensile strain, the VI_6 octahedra undergo a compressive distortion along its local (111) axis, i.e., the crystallographic c axis. As a result, the a_{1g} singlet will further split off and gets lower

in energy than the e'_{\pm} doublet. Then, the energetically more favorable $a_{1g}^1 e'_{\pm}^1$ state than e'_{\pm}^2 would turn into the insulating $a_{1g}^1 e'_{-}^1$ ground state (upon +SOC and +U), which is most desirable for the VI_3 monolayer. Indeed, the stability of the $a_{1g}^1 e'_{-}^1$ ground state against the e'_{\pm}^2 is enhanced upon the tensile strain on the optimized lattice, see the blue curve in the inset of Fig. 4. Moreover, the FM superexchange strength rises in the feasible strain (e.g., up to 5%), see the red curve. Assuming a feasible biaxial tensile strain, and using the increasing FM superexchange strength and Ising magnetism both associated with the robust $a_{1g}^1 e'_{-}^1$ ground state, we carry out Monte Carlo simulations to estimate T_C in the 2D Ising FM VI_3 monolayer. As seen in Fig. 4, T_C can be increased from 70 K for the bare VI_3 monolayer to 90 K at 2.5% strain, and to 110 K at 5.0% strain. Therefore, VI_3 monolayer could be the first Ising type 2D FM with a pretty high T_C , particularly under a biaxial tensile strain. This prediction may call for a prompt experimental verification.

In summary, 2D FM materials are desirable for spintronics. Here we have demonstrated, through DFT calculations (LSDA+SOC+U) and crystal field level analyses, that VI_3 monolayer has the $a_{1g}^1 e'_{-}^1$ ground state with a significant SIA. This unique spin-orbital ground state produces an Ising type FM via the SOC and superexchange. We have provided a picture to explain the enhanced FM superexchange in the $a_{1g}^1 e'_{-}^1$ ground state. Our results well account for the experimental hard perpendicular FM in bulk VI_3 . Moreover, we predict, based on the Monte Carlo simulations, that VI_3 monolayer could well be the first 2D Ising FM with a pretty high T_C , particularly under a biaxial tensile strain. This prediction would be worth a prompt experimental verification.

This work was supported by the NSF of China (Grants No. 11674064, No. 11704153, and No. 11474059) and by the National Key Research and Development Program of China (Grant No. 2016YFA0300700). D. I. K. was supported by the Deutsche Forschungsgemeinschaft through SFB 1238 (project number 277146847).

* Corresponding author. wuh@fudan.edu.cn

- [1] B. Huang, G. Clark, E. Navarro-Moratalla, D. R. Klein, R. Cheng, K. L. Seyler, D. Zhong, E. Schmidgall, M. A. McGuire, D. H. Cobden, W. Yao, D. Xiao, P. Jarillo-Herrero, and X. Xu, *Nature* **546**, 270 (2017).
- [2] C. Gong, L. Li, Z. Li, H. Ji, A. Stern, Y. Xia, T. Cao, W. Bao, C. Wang, Y. Wang, Z. Q. Qiu, R. J. Cava, S. G. Louie, J. Xia, and X. Zhang, *Nature* **546**, 265 (2017).
- [3] Y. Deng, Y. Yu, Y. Song, J. Zhang, N. Z. Wang, Z. Sun, Y. Yi, Y. Z. Wu, S. Wu, J. Zhu, J. Wang, X. H. Chen, and Y. Zhang, *Nature* **563**, 94 (2018).
- [4] B. Huang, G. Clark, D. R. Klein, D. MacNeill, E. Navarro-Moratalla, K. L. Seyler, N. Wilson, M. A.

- McGuire, D. H. Cobden, D. Xiao, W. Yao, P. Jarillo-Herrero, and X. Xu, *Nat. Nanotechnol.* **13**, 544 (2018).
- [5] S. Jiang, J. Shan, and K. F. Mak, *Nat. Mater.* **17**, 406 (2018).
- [6] Z. Sun, Y. Yi, T. Song, G. Clark, B. Huang, Y. Shan, S. Wu, D. Huang, C. Gao, Z. Chen, M. McGuire, T. Cao, D. Xiao, W. Liu, W. Yao, X. Xu, and S. Wu, *Nature* **572**, 497 (2019).
- [7] C. Huang, J. Feng, F. Wu, D. Ahmed, B. Huang, H. Xiang, K. Deng, and E. Kan, *J. Am. Chem. Soc.* **140**, 11519 (2018).
- [8] M. Gibertini, M. Koperski, A. F. Morpurgo, and K. S. Novoselov, *Nat. Nanotechnol.* **14**, 408 (2019).
- [9] T. Song, X. Cai, M. W. Tu, X. Zhang, B. Huang, N. P. Wilson, K. L. Seyler, L. Zhu, T. Taniguchi, K. Watanabe, M. A. McGuire, D. H. Cobden, D. Xiao, W. Yao, and X. Xu, *Science* **360**, 1214 (2018).
- [10] M. A. McGuire, H. Dixit, V. R. Cooper, and B. C. Sales, *Chem. Mater.* **27**, 612 (2015).
- [11] H. Wang, F. Fan, S. Zhu, and H. Wu, *Europhys. Lett.* **114**, 47001 (2016).
- [12] J. L. Lado and J. Fernández-Rossier, *2D Mater.* **4**, 035002 (2017).
- [13] D. H. Kim, K. Kim, K. T. Ko, J. Seo, J. S. Kim, T. H. Jang, Y. Kim, J. Y. Kim, S. W. Cheong, and J. H. Park, *Phys. Rev. Lett.* **122**, 207201 (2019).
- [14] T. Kong, K. Stolze, E. I. Timmons, J. Tao, D. Ni, S. Guo, Z. Yang, R. Prozorov, and R. J. Cava, *Adv. Mater.* **31**, 1808074 (2019).
- [15] S. Son, M. J. Coak, N. Lee, J. Kim, T. Y. Kim, H. Hamidov, H. Cho, C. Liu, D. M. Jarvis, P. A. C. Brown, J. H. Kim, C. H. Park, D. I. Khomskii, S. S. Saxena, and J. G. Park, *Phys. Rev. B* **99**, 041402 (2019).
- [16] S. Tian, J. F. Zhang, C. Li, T. Ying, S. Li, X. Zhang, K. Liu, and H. Lei, *J. Am. Chem. Soc.* **141**, 5326 (2019).
- [17] P. Blaha, K. Schwarz, G. Madsen, D. Kvasnicka, and J. Luitz, "Wien2k package," <http://www.wien2k.at>.
- [18] V. I. Anisimov, F. Aryasetiawan, and A. I. Lichtenstein, *J. Phys.: Condens. Matter* **9**, 767 (1997).
- [19] N. Metropolis and S. Ulam, *J. Am. Stat. Assoc.* **44**, 335 (1949).
- [20] J. He, S. Ma, P. Lyu, and P. Nachtigall, *J. Mater. Chem. C* **4**, 2518 (2016).
- [21] X. Ou, H. Wang, F. Fan, Z. Li, and H. Wu, *Phys. Rev. Lett.* **115**, 257201 (2015).
- [22] X. Ou and H. Wu, *Sci. Rep.* **4**, 4609 (2014).
- [23] G. Q. Liu, V. Antonov, O. Jepsen, and O. Andersen, *Phys. Rev. Lett.* **101**, 026408 (2008).
- [24] M. Haverkort, I. Elfimov, L. Tjeng, G. Sawatzky, and A. Damascelli, *Phys. Rev. Lett.* **101**, 026406 (2008).
- [25] S. Grimme, *J. Comput. Chem.* **27**, 1787 (2006).
- [26] X. Li and J. Yang, *J. Mater. Chem. C* **2**, 7071 (2014).
- [27] D. I. Khomskii, *Transition Metal Compounds* (Cambridge University Press, 2014).

Supplementary Material to “VI₃: a 2D Ising ferromagnet”

I. Cleavage Energy

To explore the possibility to exfoliate a monolayer from the bulk VI₃, we have calculated the total energy of a VI₃ bilayer as a function of the interlayer distance (see Fig. S1), using DFT+vdW corrections within the Grimme’s approach. The calculated cleavage energy of 0.27 J/m² is well comparable to those for other 2D materials such as CrI₃ (0.30 J/m²), Cr₂Si₂Te₆ (0.35 J/m²), and Cr₂Ge₂Te₆ (0.38 J/m²). Therefore, an exfoliation of VI₃ monolayer is likely.

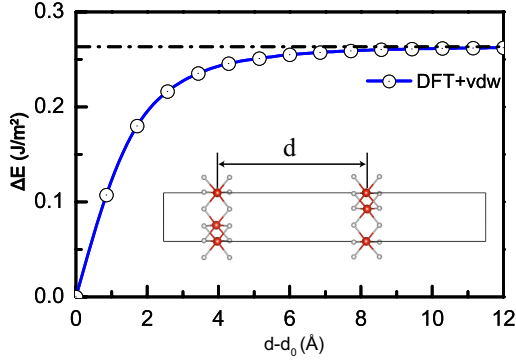


FIG. S1. The relative total energy calculated as a function of the distance between two VI₃ monolayers with a reference to the experimental vdW distance d_0 . The cleavage energy is estimated to be 0.27 J/m².

II. LDA, LSDA, and LSDA+U results

We carry out spin-restricted LDA calculations to estimate the crystal (ligand) field splitting in VI₃ monolayer. The calculated density of states (DOS) results are shown in Fig. S2. A t_{2g} - e_g like octahedral crystal field splitting of more than 1 eV makes the empty e_g states of no concern. Note that in the actual trigonal crystal field, the t_{2g} triplet splits into the nearly degenerate a_{1g} singlet and e'_{\pm} doublet, both of which are on average 1/3 filled to fulfill the formal V³⁺ $3d^2$ state. When the spin-polarized LSDA calculations are performed, we obtain a FM metallic solution (Fig. S3) with the total spin moment of 2 μ_B /fu indicative of the formal V³⁺ $S=1$ state. The V³⁺ ion has the local spin moment of 1.85 μ_B (see Table S1), and due to the strong covalency, each iodine becomes negatively spin polarized and has a local spin moment of $-0.05 \mu_B$, and the interstitial region also contributes a large spin moment of 0.3 μ_B /fu. Obviously, this metallic solution contradicts the experimental FM insulating behavior. Note that the t_{2g} -like bandwidth is less than 1 eV (Figs. S2 and S3) and should be smaller

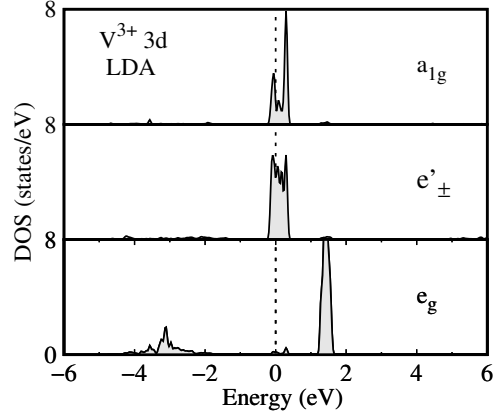


FIG. S2. V 3d DOS for VI₃ monolayer by LDA. Fermi level is set at zero energy.

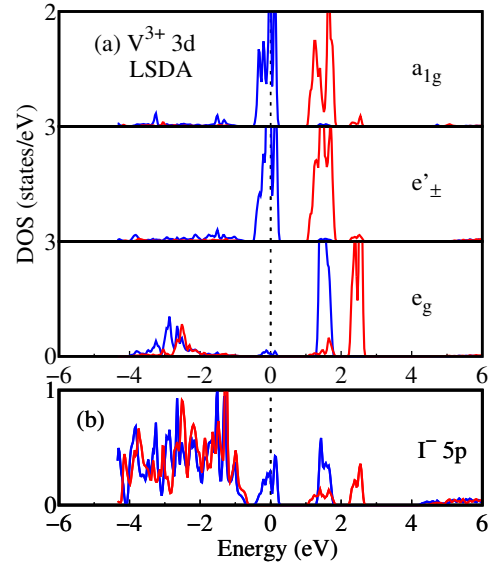


FIG. S3. V 3d and I 5p DOS by LSDA. The blue (red) curves stand for the up (down) spin channel. Fermi level is set at zero energy.

than any realistic U value of about 3-4 eV for V 3d electrons. Therefore, the electronic correlations should be taken into account, as done in the following +U calculations.

TABLE S1. Relative total energies ΔE (meV/fu) and local spin moments (μ_B) for the V³⁺ ion. The corresponding data for the fully relaxed structures are listed in the round brackets.

VI ₃ monolayer		ΔE	M_{spin}
LSDA	FM	0.0 (0.0)	1.85 (1.77)
LSDA+U	$a_{1g}^1 e'_{\pm}^1$	FM 229.6 (193.7)	2.02 (1.98)
LSDA+U	e'_{\pm}^2	FM 0.0 (0.0)	1.82 (1.77)
	AF	7.2 (7.2)	1.80 (1.75)

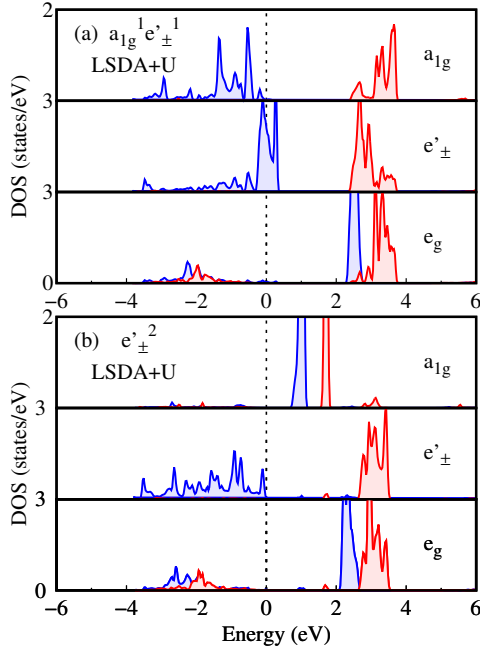


FIG. S4. (a) The metallic $a_{1g}^1 e'_{\pm}^1$ state and (b) the insulating e'_{\pm}^2 state by LSDA+U. The blue (red) curves stand for the up (down) spin channel. Fermi level is set at zero energy.

Our LSDA+U calculations give two different solutions: the metallic one ($a_{1g}^1 e'_{\pm}^1$) with the half-filled e'_{\pm}^1 state and the insulating one with the fully occupied e'_{\pm}^2 configuration, see Fig. S4. The former solution has a sharp DOS peak at the Fermi level, and therefore it meets the scenario of a Stoner FM instability. As a result, this solution may be named an itinerant FM, which is, however, in disagreement with the experimental FM insulating behavior. Actually, our LSDA+U calculations find that this solution with the high DOS peak at the Fermi level is much less stable than the insulating e'_{\pm}^2 state by 229.6 meV/fu, see Table S1. Moreover, the insulating e'_{\pm}^2 state turns out to be more stable in FM state than in the AF state by 7.2 meV/fu.